Global Sea Surface Cyclogeostrophic Currents Derived From Satellite Altimetry Data

Yuhan Cao, Changming Dong, Alexandre Stegner, Brandon J. Bethel, Chunyan Li, Jihai Dong, Haibin Lü, Jingsong Yang

JGR Oceans

RESEARCH ARTICLE
10.1029/2022JC019357

Key Points:

- An iterative method is used to cyclostrophic-correct global sea surface velocities from Archiving, Validation and Interpolation of Satellite Oceanographic Data-gridded altimetry
- The impact of curvature on the ocean currents can be seen in the dynamics of meandering, boundary currents and eddy-rich regions
- Maximum spatial differences in eddy kinetic energy and enstrophy (15%) is significantly greater than the strain rate (10%)

Correspondence to:
C. Dong and J. Dong,
cmdong@nuist.edu.cn;
jihai_dong@nuist.edu.cn

Citation:
Cao, Y., Dong, C., Stegner, A., Bethel, B. J., Li, C., Dong, J., et al. (2023). Global sea surface cyclogeostrophic currents derived from satellite altimetry data. *Journal of Geophysical Research: Oceans*, *128*, e2022JC019357. https://doi.org/10.1029/2022JC019357

Received 2 OCT 2022
Accepted 5 JAN 2023

Author Contributions:
Conceptualization: Changming Dong
Data curation: Yuhan Cao, Jihai Dong
Funding acquisition: Changming Dong, Jingsong Yang
Investigation: Yuhan Cao
Methodology: Alexandre Stegner
Project Administration: Changming Dong
Software: Yuhan Cao
Validation: Yuhan Cao
Writing – original draft: Yuhan Cao, Changming Dong, Brandon J. Bethel, Chunyan Li
Writing – review & editing: Yuhan Cao, Changming Dong, Alexandre Stegner, Chunyan Li, Haibin Lü, Jingsong Yang

Global Sea Surface Cyclogeostrophic Currents Derived From Satellite Altimetry Data

Yuhan Cao[1,2,3], Changming Dong[1,4,5], Alexandre Stegner[6], Brandon J. Bethel[4,7], Chunyan Li[8], Jihai Dong[1,4], Haibin Lü[2], and Jingsong Yang[9]

[1]School of Marine Sciences, Nanjing University of Information Science and Technology, Nanjing, China, [2]School of Marine Technology and Geomatics, Jiangsu Ocean University, Lianyungang, China, [3]Jiangsu Key Laboratory of Marine Bioresources and Environment, Jiangsu Key Laboratory of Marine Biotechnology, Jiangsu Ocean University, Lianyungang, China, [4]Southern Marine Science and Engineering Guangdong Laboratory (Zhuhai), Zhuhai, China, [5]Department of Atmosphere and Oceanic Sciences, University of California, Los Angeles, CA, USA, [6]Laboratoire de Météorologie Dynamique, CNRS, IPSL, Ecole Polytechnique, Palaiseau, France, [7]Small Island Sustainability, University of The Bahamas, Nassau, The Bahamas, [8]Department of Oceanography and Coastal Sciences, College of the Coast and Environment, Louisiana State University, Baton Rouge, LA, USA, [9]State Key Laboratory of Satellite Ocean Environment Dynamics, Second Institute of Oceanography, Ministry of Natural Resources, Hangzhou, China

Abstract Sea surface currents (SSC) derived from the sea surface height anomalies (SSHA) as measured by multi-satellite altimeters are widely used for various applications including studies on ocean dynamics, marine ecology, and climate change. However, present SSC products estimated on the assumption of an idealized geostrophic balance is biased. To overcome this idealization, this study considers flow curvature in the estimation of sea surface velocities in the global ocean, with the computation scheme validated using numerical model results. It is demonstrated that the inclusion of curvature into SSC estimations significantly changes SSC dynamic features in terms of kinetic energy, enstrophy (the maximum spatial difference is about 15%), and strain rate (the maximum spatial difference is about 10%). Such correction is of importance to the application studies relying on the SSC products from the satellite measured SSHA.

Plain Language Summary Sea surface currents (SSC) are usually derived from satellite altimetry measurements based on the balance between the pressure gradient and Coriolis effect, that is, geostrophic approximation. In this study, it is presented for the first time that the effect of flow curvature is considered in the calculation of the SSC for the global ocean using the satellite remote sensing sea surface height anomalies. Such correction is significant in terms of eddy kinetic energy, enstrophies and strains. The results show that maximum spatial differences in eddy kinetic energy and enstrophy (15%) is significantly greater than the strain rate (10%). In addition, it is of great significance for cyclostrophic-correcting the surface geostrophic velocities derived from altimeters in meandering, boundary currents and eddy-rich regions.

1. Introduction

Satellite altimeters are valuable tools for exploring and monitoring the state of the ocean. It is one of the most effective methods for global observations of ocean surface parameters such as sea surface height anomalies (SSHA) and sea surface currents (SSC) fields (Andres et al., 2008; Chelton et al., 2007; Imawaki et al., 2001; Xu et al., 2019). SSC fields are the geostrophic currents derived from SSHAs based on the geostrophic balance approximation (GBA) between the pressure gradient force and Coriolis force. Remote sensing images reveal that the ocean is full of curved currents (Abernathey et al., 2010; Chelton et al., 2007, 2011; Zhang et al., 2019). When a fluid bends and rotates, the effect of the centrifugal force is significant, especially for the nonlinear vortex rotating at high speed and accompanied by strong shearing (Douglass & Richman, 2015). The degree of flow bending can be described by the curvature. The curvature radius of the flow is closely related to the first baroclinic Rossby deformation radius, which plays an important role in the ocean (Cushman-Roisin & Beckers, 2011).

The classical geostrophic balance theory ignores the effect of centrifugal force on the real sea motion, which makes the flow field, especially true for curved flow in mesoscale ocean eddies, measured by the altimeter has certain errors under the assumption of geostrophic balance (Buckingham et al., 2021; Maximenko & Niiler, 2006; Zhang et al., 2019). Mesoscale eddies are ubiquitous in the global ocean and play important roles in transporting matter, heat and momentum (Chelton et al., 2011; C. Dong et al., 2014; Ji et al., 2018; Liu et al., 2017),

but also, when intense, eddies and meandering jets may render the GBA approximation invalid (Douglass & Richman, 2015; Ioannou et al., 2019; Penven et al., 2014). This is because the approximation ignores the curvature of streamlines, and this is a nonlinear term in the momentum equation, thereby introducing errors in flow field estimations (Maximenko & Niiler, 2006).

How to produce estimations of SSCs based on GBA with flow curvatures included into calculations has long attracted the interest of oceanographers (Buckingham et al., 2021; Shakespeare, 2016; Wenegrat & Thomas, 2017), but it should be noted that it is different from the velocity correction of the non-geostrophic velocity component, Ekman flows, caused by surface wind stress (Douglass & Richman, 2015; Fratantoni, 2001; Ioannou et al., 2019; Penven et al., 2014; Uchida & Imawaki, 2003; Uchida et al., 1998). So far, three methods have been proposed to correct geostrophic velocities derived from merged satellite altimeter data: gradient wind equation (Ioannou et al., 2019; Penven et al., 2014; Qiu et al., 2019), perturbation expansion (Penven et al., 2014) and an iterative method (Ioannou et al., 2019; Penven et al., 2014). When estimating surface currents derived from SSHAs, the cyclogeostrophic balance is often used but it is only when calculating axisymmetric and compact eddies with a constant curvature radius (Douglass & Richman, 2015), and as such, amongst the aforementioned methods, the perturbation method is least accurate in most situations due to its reliance on small values of the Rossby number (*Ro*) (Penven et al., 2014). The iterative method makes small corrections each step to the SSC to consider the influence of centrifugal acceleration caused by local curvature on the geostrophic velocity. The iterative method has been successfully applied to a large ring in the Mozambique Channel (Penven et al., 2014) and mesoscale eddies in the Mediterranean Sea (Ioannou et al., 2019).

In this study, we apply the iterative method to correct the 1993–2018, 26-year global daily geostrophic velocity fields derived by Archiving, Validation and Interpolation of Satellite Oceanographic Data (AVISO). It is found that the differences between the corrected currents and the original geostrophic currents are significant, especially for intense mesoscale eddy regions and western boundary current regions in terms of global eddy kinetic energy (EKE), enstrophy (ENS), strain rate (S), and relative vorticity. The paper is organized as follows: the methods and data used in this study are described in Section 2. In Section 3, the main results including the validation of correction scheme and the temporal-spatial variation of differences between the cyclogeostrophic currents and original geostrophic currents are explored. The effects of curvature on the oceanic surface currents are discussed in Section 4, and the summary is given in Section 5.

2. Data and Methods

2.1. Data

2.1.1. Satellite Data

Global geostrophic velocity fields derived from the National Centre for Space Studies (CNES; French: Centre National D'Études Spatiales)'s Archiving Validation and Interpolation of Satellite Oceanographic (AVISO) multi-satellite merged altimeter data product is used in this study (updated 17 January 2019), and is composed of the Data Unification and Altimeter Combination System (DUACS) (Taburet et al., 2019). The daily data used in this study with a spatial resolution of 1/4° × 1/4° are from 1 January 1993 to 31 December 2018.

2.1.2. MITgcm

The Massachusetts Institute of Technology General Circulation Model (MITgcm) is a global numerical model is the first non-hydrostatic models of the ocean. The objective of this model is to study the ocean, atmosphere and climate. It has an automatically generated adjoint that allows the model to be used for data assimilation (Marshall et al., 1997). The LLC4320 simulation, which is part of a hierarchy of MITgcm free-running simulation, is used to validate the iterative scheme. LLC indicates the Latitude-Longitude-polar Cap configuration, and 4,320 represents the number of grid points on each side of the 13 square tiles (J. Dong et al., 2021; Rocha et al., 2016; Torres et al., 2018). The LLC4320 has a horizontal resolution of 1/48° with 90 vertical z-levels over the globe and integration time step is 25 s. In this study, the hourly output of LLC4320 is used to examine the sea surface current at 1:00 a.m. (UTC) on 14 September 2011, between 25°–45°N and 142°–180°E.

2.2. Methods

2.2.1. Kinematic Parameters

2.2.1.1. Eddy Kinetic Energy (EKE)

The EKE at each grid point in space and time can be calculated from surface velocity anomaly:

$$EKE = \frac{1}{2}\left(\left(u'\right)^2 + \left(v'\right)^2\right) \tag{1}$$

where u' and v' are the surface velocity anomalies of zonal and meridional currents. The geostrophic eddy kinetic energy is obtained by the current components computed from the SSHA of AVISO/DUCAS. The cyclogeostrophic eddy kinetic energy is obtained by the cyclogeostrophic surface currents.

2.2.1.2. Enstrophy (ENS)

The enstrophy is an important dynamic parameter, defined as the square of vorticity (Cushman-Roisin & Beckers, 2011). The ENS at each grid in space and time is calculated by:

$$ENS = \frac{1}{2}\left(\frac{\partial v'}{\partial x} - \frac{\partial u'}{\partial y}\right)^2 \tag{2}$$

where the x- and y-axis are directed eastward and northward, respectively.

2.2.1.3. Strain Rate (S)

The strain rate S is related to shear deformation $\vartheta = \frac{\partial v'}{\partial x} + \frac{\partial u'}{\partial y}$ and stretching deformation $\varsigma = \frac{\partial u'}{\partial x} - \frac{\partial v'}{\partial y}$ given by:

$$S = \sqrt{\vartheta^2 + \varsigma^2} \tag{3}$$

2.2.2. Iterative Method

Mesoscale curved ocean currents are approximately in cyclogeostrophic balance (CGB), and in cylindrical coordinates, the balance can be written as:

$$\frac{V^2}{fR} + V = V_g \tag{4}$$

where f is Coriolis parameter, V is the azimuthal velocity, V_g is the geostrophic velocity determined by the pressure gradient force and R is the radius of curvature. This equation can be solved analytically for V. However, the equation has no solution for small radii (Douglass & Richman, 2015).

For surface currents, introducing geostrophic velocities, the cyclogeostrophic current equation in cartesian coordinates can be transformed as:

$$\begin{cases} u\dfrac{\partial u}{\partial x} + v\dfrac{\partial u}{\partial y} - fv = -g\dfrac{\partial \eta}{\partial x} \\ u\dfrac{\partial v}{\partial x} + v\dfrac{\partial v}{\partial y} + fu = -g\dfrac{\partial \eta}{\partial y} \end{cases} \Rightarrow \begin{cases} u\dfrac{\partial u}{\partial x} + v\dfrac{\partial u}{\partial y} - fv = -fv_g \\ u\dfrac{\partial v}{\partial x} + v\dfrac{\partial v}{\partial y} + fu = fu_g \end{cases} \tag{5}$$

where u_g and v_g are the geostrophic velocity anomalies of zonal and meridional currents, u and v are surface velocities of zonal and meridional currents, η and g are the sea surface height and gravitational acceleration parameter, respectively. In order to give the solution of the cyclogeostrophic velocity components to Equation 5 for mesoscale eddies and strong surface mean currents with different shapes, this study uses an iterative method based on Penven et al. (2014), which was commonly used in atmospheric sciences (Arnason et al., 1962) to approximately solve the CGB. The method was applied to solve the momentum equation of ocean currents under cyclogeostrophic equilibrium conditions. This iterative scheme is given by

$$\vec{u}^{(n+1)} - \frac{\vec{k}}{f} \times \left(\vec{u}^{(n)} \cdot \nabla \vec{u}^{n}\right) = \vec{u}_g \tag{6}$$

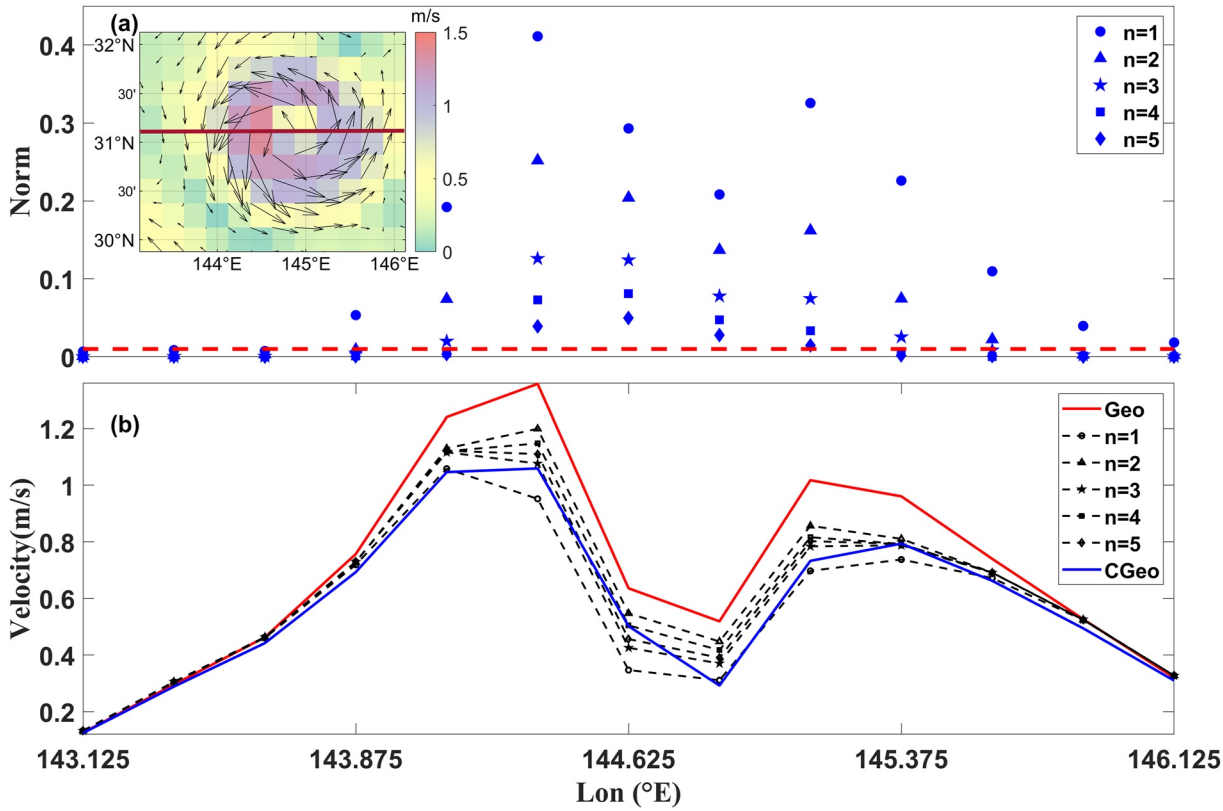

Figure 1. Iterative scheme experiment applied to northern hemisphere cyclonic eddies. (a) Changes in the norm value of each grid point on the solid red line. (b) Accuracy of the velocity of each grid point on the solid red line. The initial geostrophic velocity is plotted with solid red line; the solution of the gradient wind balance equation is plotted with solid blue line, and the ocean current velocity at each iterative step is plotted with dashed black line.

where $\vec{k}$ is the vertical unit vector, $\vec{u}$ is the surface velocity vector, and $\vec{u}_g$ is the geostrophic velocity vector. The specific iterative method is as follows:

$$
\begin{aligned}
u^{n+1} &= u_g - \frac{1}{f}\left(u^n\frac{\partial v^n}{\partial x} + v^n\frac{\partial v^n}{\partial y}\right)\\
v^{n+1} &= v_g + \frac{1}{f}\left(u^n\frac{\partial u^n}{\partial x} + v^n\frac{\partial u^n}{\partial y}\right)\\
n &= 0,\\
&\qquad u = u_g, \quad v = v_g\\
n &= 1,\\
u^{(2)} &= u_g - \frac{1}{f}\left(u_g\frac{\partial v_g}{\partial x} + v_g\frac{\partial v_g}{\partial y}\right)\\
v^{(2)} &= v_g + \frac{1}{f}\left(u_g\frac{\partial u_g}{\partial x} + v_g\frac{\partial u_g}{\partial y}\right)\\
&\cdots\cdots
\end{aligned}
\tag{7}
$$

A cyclonic eddy (Figure 1) and an anticyclonic eddy (Figure 2) with a grid resolution of 1/4° in the northern hemisphere are tested to investigate the convergence conditions of iteration. The cyclonic eddy generated from the strong west boundary current path meander on 12 August 1998 is shown in Figure 1. The maximum geostrophic velocity derived from AVISO/DUCAS altimeters at the edge of the eddy is 1.5 m/s, the radius is about 100 km, and the shape is similar to the Gaussian vortex. The velocity of each grid point at the latitude of 31.125°N (the red solid line in the small figure in Figure 1a) is selected for testing, and the norm value of each iteration (the large figure in Figure 1a) is calculated. Figure 1b shows the comparation of altimeter-derived geostrophic velocity, gradient wind velocity and iterative velocity. Figure 2 displays an anticyclonic eddy derived

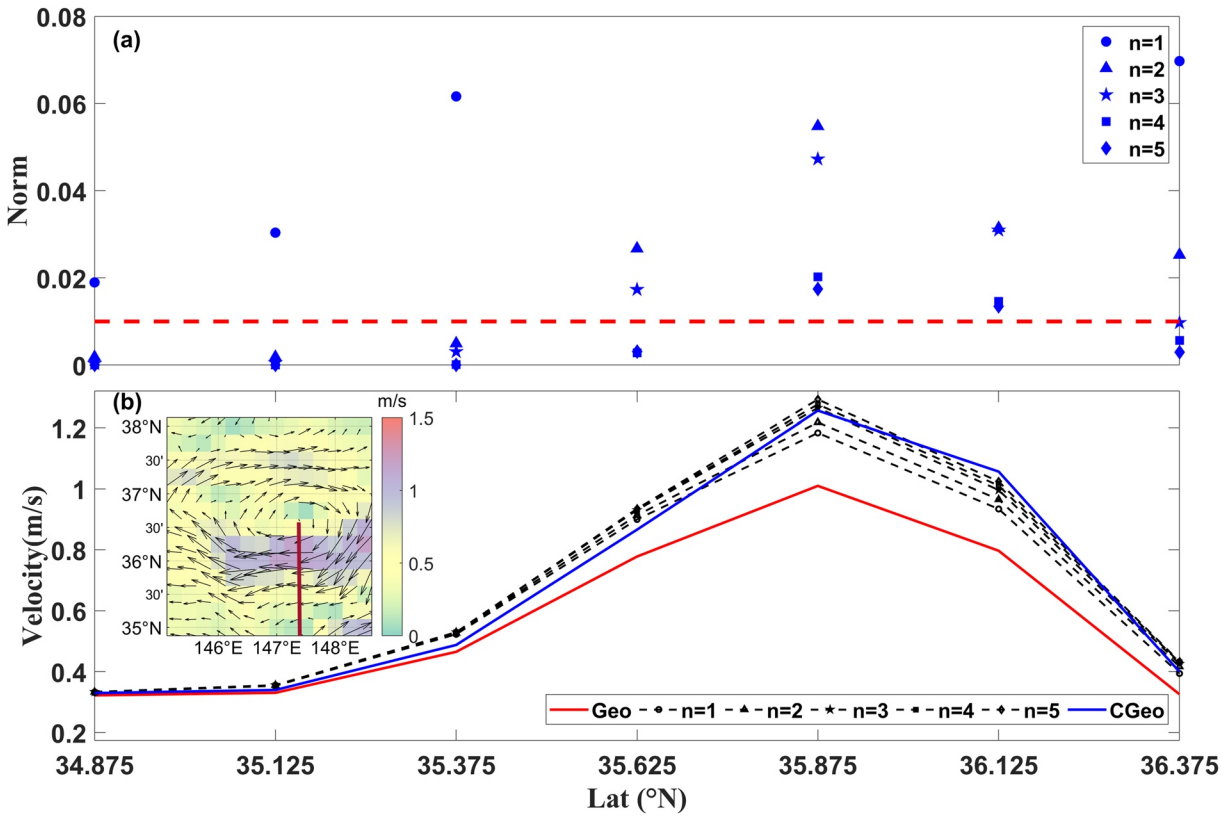

Figure 2. Same as Figure 1, but for anticyclonic eddies.

from AVISO/DUCAS on 12 June 1996. The maximum geostrophic velocity of the eddy is 1.5 m/s, and the shape is nearly elliptical. Figure 2a shows the norm value of each iteration at the longitude of 147.375°E (the red solid line in the small figure in Figure 2b) for the anticyclonic eddy. The comparation of AVISO altimeter-derived geostrophic velocity, gradient wind velocity and iterative velocity as shown in Figure 2b. The velocity transects along these structures confirm that the iterative method converges quickly toward the reference velocity field. Consequently, the scheme iterates point-by-point until the norm is below 0.01 or increases. It is worth noting that the iteration of grid points with small velocity stops after one step.

3. Results

3.1. Validation

In order to ensure the accuracy of the iterative method to correct the global geostrophic current, the iterative method is applied to the geostrophic velocities derived from the SSH of the MITgcm model. Validation of correction scheme is conducted by using model 5 m current and sea surface height fields. Two cases (a larger area that contains a meandering jet, an isolated cyclonic eddy and an anticyclonic eddy) in the Kuroshio extension are examined. First, the high-resolution model data is processed into a fine 1/4° resolution to match the altimeter data. Then, the SSC derived from sea surface height and corrected velocities are compared with the reference surface velocities (5 m) of the model.

The root-mean-square error (RMSE) of reference sea surface (5 m) velocities and surface geostrophic velocities calculated based on the sea surface heights (iterative scheme-estimated cyclogeostrophic velocities) from the MITgcm model is 0.13 m/s (0.11 m/s) from 33°–38°N and 146°–153°E (Figures 3a–3c). Similarly, the RMSE of the velocity based on the cyclogeostrophic profiles is 0.11 m/s and here it should be noted that the cyclogeostrophic RMSE is 38% lower than the geostrophic one (0.18 m/s). Figures 3d–3f show that the RMSE of simulated sea surface velocities and surface geostrophic velocities (cyclogeostrophic velocity) is 0.18 m/s (0.17 m/s) from 37°–40°N and 153°–157°E. In the northeast side of the anticyclonic eddy where *Ro* is large, the cyclogeostrophic

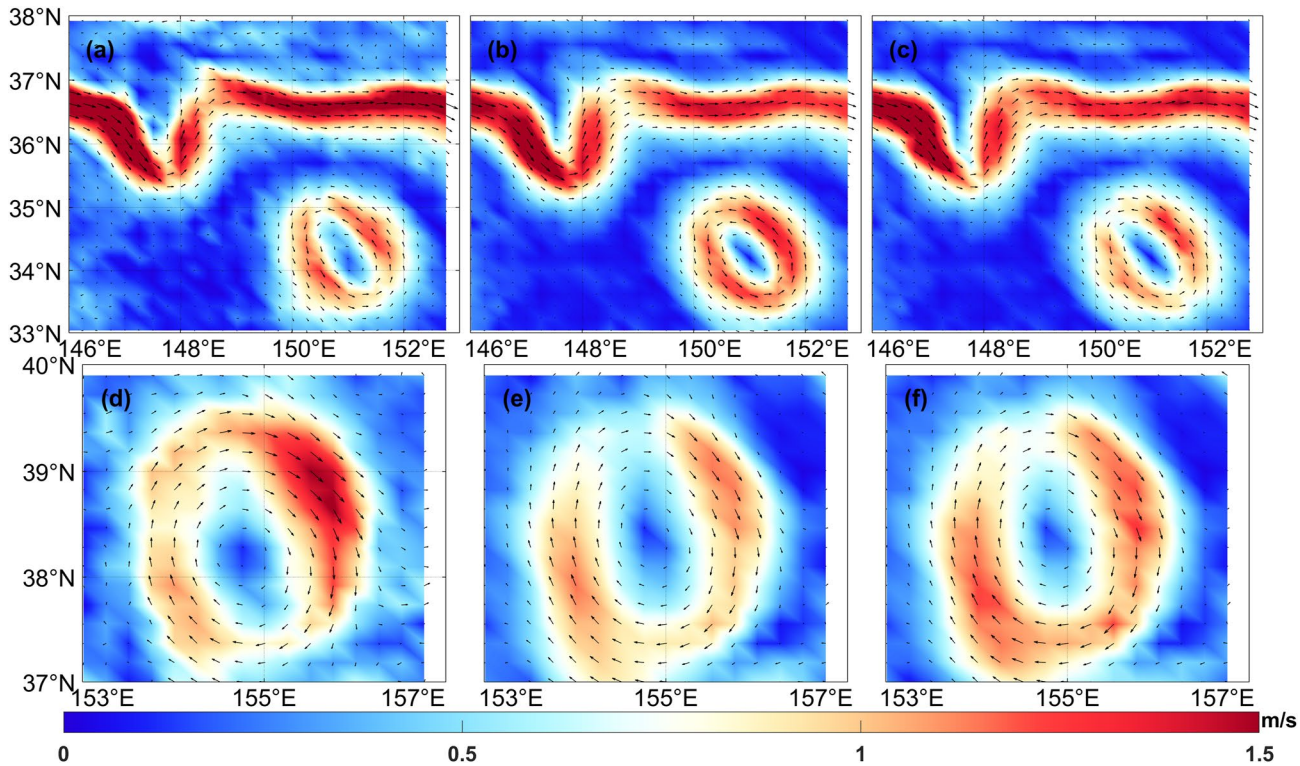

Figure 3. (a) Sea surface (5 m) velocity simulated by the MITgcm model of a cyclonic eddy and a section of jets. (b) Surface geostrophic velocity calculated based on the sea surface height in the model data for a cyclonic eddy and a section of jets. (c) Cyclogeostrophic velocities, calculated by the iterative scheme for the sea surface height, are shown in the right panels for a cyclonic eddy and a section of jets. (d–f) Same as (a–c), but for an anticyclonic eddy. The background color indicates the velocity (unit: m/s) and the vectors indicate the direction.

RMSE is 10% lower than the geostrophic one. Through the above verification tests, it shows that the iterative scheme in this paper is feasible.

3.2. Comparation of Global Geostrophic and Cyclogeostrophic Surface Currents

For the global ocean, the climatic normalized differences between global geostrophic EKE (Equation 1) and cyclogeostrophic EKE are relatively large in regions where the currents are strong (Figure 4a). This is the case, for example, along western boundary current systems (e.g., the Kuroshio and Gulf Stream) and the Subtropical Countercurrent, as shown by the global distribution of cyclogeostrophic EKE in Figure 4b. The climatic cyclogeostrophic ENS of these regions are similarly energetic. The regional eddy-eddy and eddy-mean flow interactions are strong (Figure 4c), and the normalized differences of multi-year average between global geostrophic ENS (Equation 2) and cyclogeostrophic ENS are large (Figure 4d). Figures 4e and 4f show the variation of another important parameter: the strain rate. The spatial characteristics of normalized differences between global geostrophic S (Equation 3) and cyclogeostrophic S are similar to the EKE distribution (Figure 4e). However, the differences are smaller than in the first two energy parameters.

Cyclogeostrophic corrections greatly affect the curved meanders of the major boundary currents. The spatial differences between the initial and adjusted current fields show bipolar characteristics on both sides of the strong western boundary current. In the northern hemisphere, geostrophic velocities based on sea level data underestimate (overestimate) actual velocities on the north (south) side of the boundary current. The opposite conclusions hold for the southern hemisphere, but in each case, the larger the velocity, the greater the difference. The cyclogeostrophic correction increases (decreases) the intensity of strong anticyclonic (cyclonic) eddies (Ioannou et al., 2019). As expected, we found that areas where anticyclone (cyclones) dominates the ocean circulation exhibit a positive (negative) difference of about 16.38% (−14.21%) as shown in Figure 4.

To better understand the relationship between the difference and the relative vorticity of ocean current, the interannual temporal variation of global area-weighted average (excluding 15°S–15°N) EKE, ENS, and S of the

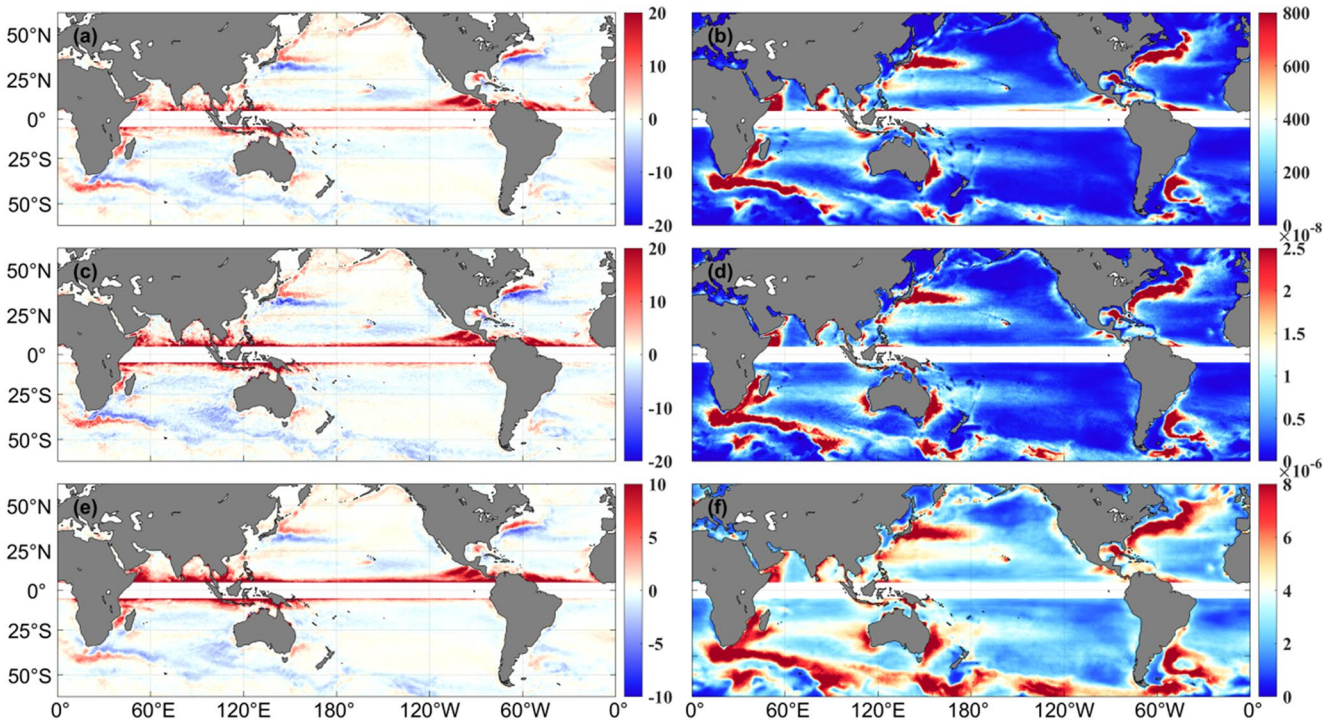

Figure 4. Global climatic (a) normalized difference between geostrophic EKE and cyclogeostrophic EKE, (b) distribution of cyclogeostrophic EKE (cm^2/s^2), (c) normalized difference between geostrophic enstrophy and cyclogeostrophic enstrophy, (d) Global climatic distribution of cyclogeostrophic enstrophy (m^2/s^2), (e) normalized difference between multi-year average global geostrophic strain rate and cyclogeostrophic strain rate, and (f) distribution of cyclogeostrophic strain rate (s^{-1}).

positive (cyclonic) and negative relative vorticity (anticyclonic) currents are investigated. Figure 5a displays the time series of global area-weighted average EKE. It is found that cyclogeostrophic EKE is lower than geostrophic cyclonic EKE, with a difference of about 8.7%. Inversely, cyclogeostrophic EKE is larger than geostrophic anticyclonic EKE (with a difference of about 9%). The same difference is also seen in ENS that possess a maximum difference of −11.3% (12.7%) for cyclones (anticyclones) (Figure 5b). Figure 5c shows the interannual temporal variation of strain rate from 1993 to 2018. There is a similar difference characteristic in S. However, the difference of S is noticeably smaller than that of the first two dynamic parameters (with a difference of about 2%).

4. Discussion

In the ocean, currents with curved shapes are ubiquitous. Under the GBA when the *Ro* is expected to be much less than one, the Coriolis force is approximately balanced by the pressure gradient force. Douglass and Richman (2015) and Ioannou et al. (2019) have demonstrated that cyclogeostrophic correction is needed for mesoscale eddies with the *Ro* larger than 0.1. When *Ro* is large, the dynamics are nonlinear and non-quasigeostrophic (Cushman-Roisin & Beckers, 2011). The significance of curvature in the SSC can be determined from the ratio of the cyclogeostrophic Rossby number (Ro_c) (Shakespeare, 2016). According to Equation 4, the Ro_c can be given by:

$$Ro_c = \frac{V}{fR} = \frac{V_g - V}{V} \tag{8}$$

Figure 6a shows the global distribution of the Ro_c of the multi-year average surface currents. It is found that the effect of curvature is important when Ro_c is higher than 0.05. The values of Ro_c in the subtropics, Gulf Stream, Kuroshio, and Antarctic Circumpolar Current regions are large. The spatial pattern of Ro_c is similar to the normalized difference between geostrophic and cyclogeostrophic dynamic parameters. In other words, curvature is the main reason for the difference. Force analysis of cyclogeostrophic balance for curved currents in the northern hemisphere (Figure 6b) shows that when fluid particle moves along a cyclonic path ($fv > 0$), the Coriolis force points outward along the radius of curvature and the pressure gradient force points toward the center of the circle.

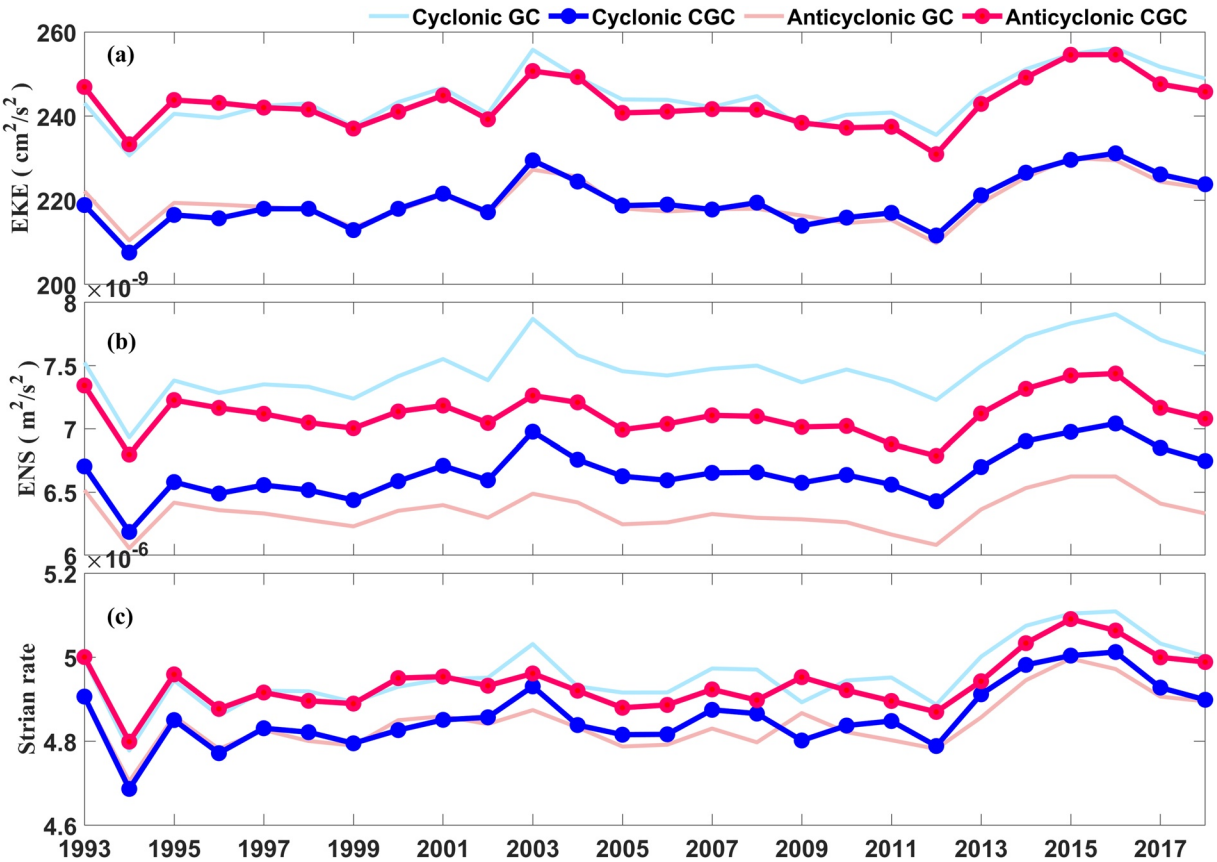

Figure 5. Time series of inter-annual variation of area-weighted averaged (a) EKE, (b) enstrophy, and (c) strain rate during 1993–2018. The dotted blue and red lines represent geostrophic cyclonic and anticyclonic currents, respectively. The solid light blue and red lines represent the cyclogeostrophic cyclonic and anticyclonic currents, respectively.

A net centripetal force toward the center of the circle (or a reduced Coriolis force) is required for a leftward turn. This leftward turn is accompanied by a deceleration or an increase in acceleration toward the center of the circle. Similarly, when a fluid particle moves in an anticyclonic motion ($fv < 0$), the Coriolis force points to the center of the circle and the pressure gradient force points outward along the radius of curvature. For curved current, it is necessary to provide a net centripetal force pointing to the center of the circle, leading to increases in the Coriolis force, that is, increasing the flow velocity or increase the acceleration pointing outward along the radius of curvature, as shown in Figure 6b. The curvature discussed is due to the flow in different bending directions, and the direction of the centripetal force that causes the flow to bend is also different.

From the above discussion (Equations 4 and 8), it has been concluded that the differences between the geostrophic and cyclogeostrophic currents, that is, the errors carried by the geostrophic currents, depends on the curvature κ:

$$\kappa = \frac{f(V_g - V)}{V^2} \tag{9}$$

Altimetry data with high resolution can resolve smaller eddies and finer structures with larger curvature, therefore, errors which are carried by the geostrophic currents derived from high-resolution altimetry data are larger.

To quantify the conclusion, we use the high-resolution numerical results with the resolution (1/48°) of the MITgcm model by subsampling the data from 1/2°, 1/4°, 1/6°, 1/8°, 1/12° to 1/24°. The relative differences in the velocities derived from modeled-SSH compared with the cyclogeostrophic correcting velocities with the different resolution, from 1/2° to 1/24°, are quantified (Figure 7). The tested region ranges from 32° to 36°N in latitude and from 150° to 156°E in longitude. Figure 7 shows that the relative differences of average velocity difference between the geostrophic and cyclogeostrophic currents with respective to the cyclogeostrophic currents vary with the resolution. The finer the spatial resolution is, the greater the relative difference of average velocity is.

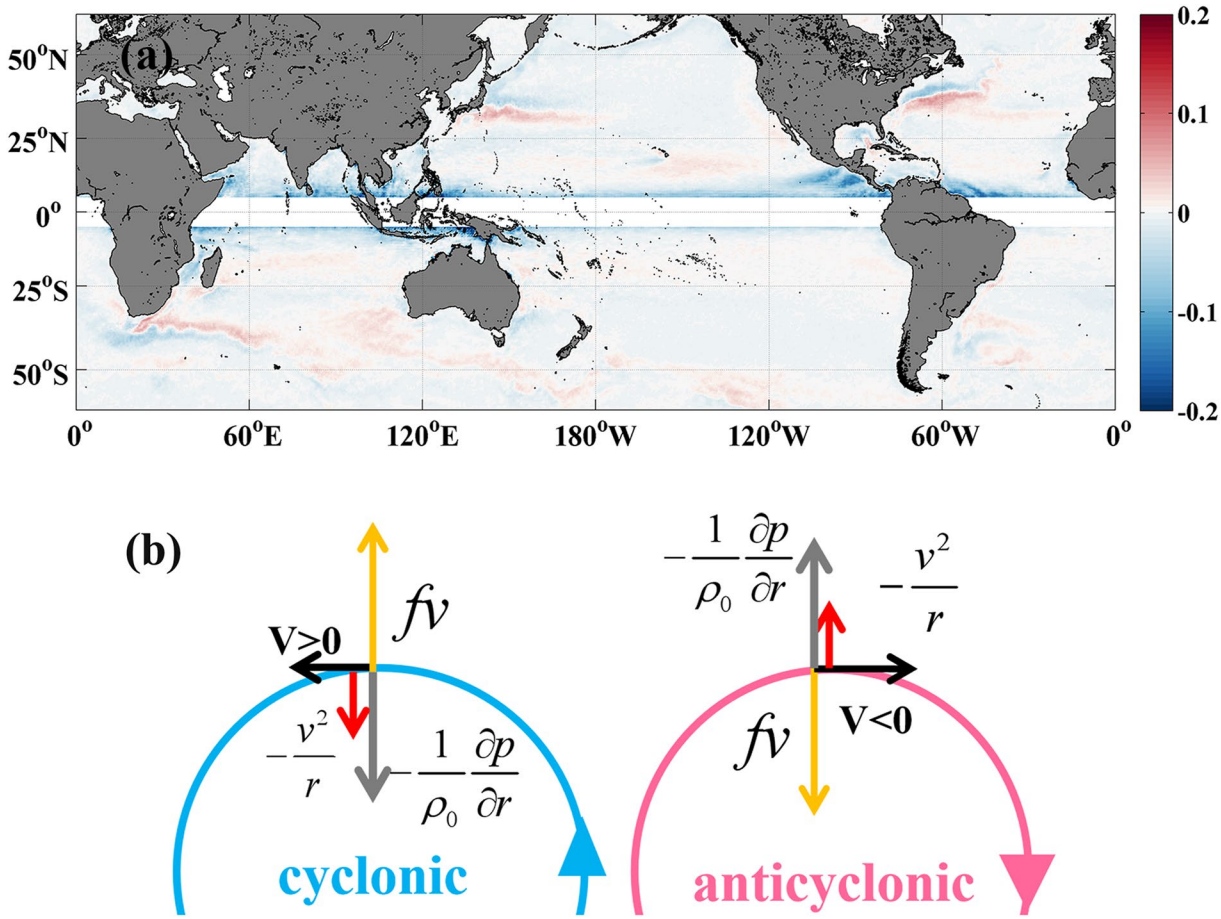

Figure 6. (a) Global distribution of cyclogeostrophic Rossby number of the multi-year average intense surface currents. (b) Schematic of the dynamic process of the curved surface current in the northern hemisphere under cyclogeostrophic balance.

The maximum (minimum) mean relative difference of is 22.6% (4.4%) at the grid resolutions of 1/24° (1/2°). The mean relative difference of velocity increases exponentially with the data resolution. It might imply that more cautions should be taken when the geostrophic currents are derived from the SSH data from the successful launch of Surface Water and Ocean Topography (SWOT) mission and the present method can be applied to the correction.

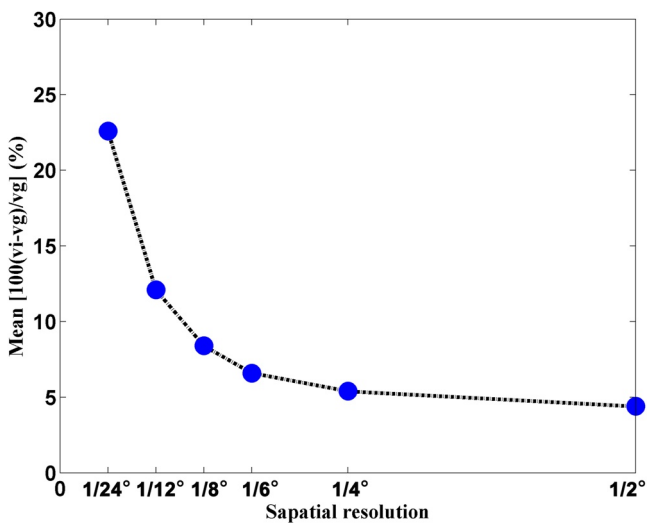

Figure 7. Variations in the mean relative differences of velocities with the resolution of the model data.

5. Conclusions

With the development of ocean observation and numerical simulation technology, the ubiquitous mesoscale and small-scale bending flow phenomenon in the ocean have been revealed. Unlike rectilinear flow, the inertial centrifugal force associated with the radius of curvature is important for curvilinear flow. Especially for a meandering jet or circular eddies, and for flows with the *Ro* approaching unity (Cushman-Roisin & Beckers, 2011). More field observations of mesoscale eddies show that eddies in high latitude seas mostly satisfy cyclogeostrophic balance (Qiu et al., 2019; Scott et al., 2019; Timmermans et al., 2008; Zhao et al., 2014). This study shows that cyclogeostrophic correction of the global surface current derived from the altimeter is necessary. The iterative method can give the effective cyclostrophic correction at global surface current. Combined with ocean model MITgcm, the accuracy of the iterative method has been assessed. The

application of model data contributes to the determination of the convergence conditions of the iterative method for correcting the altimeter global surface current.

Using the iterative method to correct the 26-year surface geostrophic currents from the AVISO products, it was found that a substantial improvement in the estimation of surface velocities was achieved. The difference between the cyclogeostrophic currents and original geostrophic currents are compared to demonstrate the significance of the correction. The flow curvature plays an important role in the eddy-rich regions. Moreover, the statistical analysis shows that the cyclogeostrophic correction strongly impacts the highly energetic midlatitude and subtropical regions. The effect of curvature on the dynamics of anticyclonic currents are more significant than that in cyclonic current. By analyzing the temporal and spatial differences of EKE, ENS, and strain rate of global ocean surface geostrophic and cyclogeostrophic currents, it is found that the difference in EKE and ENS (maximum spatial difference of 15%) is significantly greater than that in strain rates (maximum spatial difference of 10%).

The cyclogeostrophic Rossby number is investigated based on the GWB. The higher Ro_c is mainly distributed in the highly energetic midlatitude and subtropical regions. Curvature in these regions modifies the balanced state of the curved current from geostrophic balance to cyclogeostrophic balance. The impact of curvature on the ocean currents can be seen in the dynamics of meandering, boundary currents and eddy-rich regions.

The results of this study highlight the effect of curvature on the surface current velocities. Our investigation here has corrected global altimetry surface geostrophic velocities at 1/4° resolution, but the role of curvature is more critical when higher resolution altimeters are available. Our results help to better promote the study of the role of curvature in ocean current dynamics.

Data Availability Statement

The AVISO/DUACS 2018 altimeter data used in this study are available from the Copernicus Marine Service (https://resources.marine.copernicus.eu/product-detail/SEALEVEL_GLO_PHY_L4_MY_008_047/INFORMATION). The product can access from https://doi.org/10.48670/moi-00148. Downloading altimeter satellite gridded data for free need to follow the data policy of the Copernicus Marine Service. The LLC4320 data can be directly accessed from the ECCO Data Portal (https://data.nas.nasa.gov/ecco/data.php).

Acknowledgments
This study is supported by the National Natural Science Foundation of China, Grant 42250710152; the Research Startup Foundation of Jiangsu Ocean University, Grant KQ22012; the Southern Marine Science and Engineering Guangdong Laboratory (Zhuhai), Grant SML2020SP007; This study is also funded by the Priority Academic Program Development of Jiangsu Higher Education Institutions (PAPD).

References

Abernathey, R., Marshall, J., Shuckburgh, E., & Mazloff, M. (2010). Enhancement of mesoscale eddy stirring at steering levels in the Southern Ocean. *Journal of Physical Oceanography*, *40*(1), 170–185. https://doi.org/10.1175/2009jpo4201.1

Andres, M., Park, J. H., Wimbush, M., Zhu, X. H., Chang, K. I., & Ichikawa, H. (2008). Study of the Kuroshio/Ryukyu Current system based on satellite-altimeter and in situ measurements. *Journal of Oceanography*, *64*(6), 937–950. https://doi.org/10.1007/s10872-008-0077-2

Arnason, G., Haltiner, G. J., & Frawley, M. J. (1962). Higher-order geostrophic wind approximations. *Monthly Weather Review*, *90*(5), 175–185. https://doi.org/10.1175/1520-0493(1962)090<0175:hgwa>2.0.co;2

Buckingham, C. E., Gula, J., & Carton, X. (2021). The role of curvature in modifying frontal instabilities. Part I: Review of theory and presentation of a nondimensional instability criterion. *Journal of Physical Oceanography*, *51*(2), 299–315. https://doi.org/10.1175/jpo-d-19-0265.1

Chelton, D. B., Schlax, M. G., & Samelson, R. M. (2011). Global observations of nonlinear mesoscale eddies. *Progress in Oceanography*, *91*(2), 167–216. https://doi.org/10.1016/j.pocean.2011.01.002

Chelton, D. B., Schlax, M. G., Samelson, R. M., & de Szoeke, R. A. (2007). Global observations of large oceanic eddies. *Geophysical Research Letters*, *34*(15). https://doi.org/10.1029/2007gl030812

Cushman-Roisin, B., & Beckers, J. M. (2011). *Introduction to geophysical fluid dynamics: Physical and numerical aspects*. Academic Press.

Dong, C., McWilliams, J. C., Liu, Y., & Chen, D. (2014). Global heat and salt transports by eddy movement. *Nature Communications*, *5*(1), 1–6. https://doi.org/10.1038/ncomms4294

Dong, J., Fox-Kemper, B., Zhang, H., & Dong, C. (2021). The scale and activity of symmetric instability estimated from a global submesoscale-permitting ocean model. *Journal of Physical Oceanography*, *51*(5), 1655–1670. https://doi.org/10.1175/jpo-d-20-0159.1

Douglass, E. M., & Richman, J. G. (2015). Analysis of ageostrophy in strong surface eddies in the Atlantic Ocean. *Journal of Geophysical Research: Oceans*, *120*(3), 1490–1507. https://doi.org/10.1002/2014jc010350

Fratantoni, D. M. (2001). North Atlantic surface circulation during the 1990's observed with satellite-tracked drifters. *Journal of Geophysical Research*, *106*(C10), 22067–22093. https://doi.org/10.1029/2000jc000730

Imawaki, S., Uchida, H., Ichikawa, H., Fukasawa, M., Umatani, S. I., & ASUKA Group. (2001). Satellite altimeter monitoring the Kuroshio transport south of Japan. *Geophysical Research Letters*, *28*(1), 17–20. https://doi.org/10.1029/2000gl011796

Ioannou, A., Stegner, A., Tuel, A., Levu, B., Dumas, F., & Speich, S. (2019). Cyclostrophic corrections of AVISO/DUACS surface velocities and its application to mesoscale eddies in the Mediterranean Sea. *Journal of Geophysical Research: Oceans*, *124*(12), 8913–8932. https://doi.org/10.1029/2019jc015031

Ji, J., Dong, C., Zhang, B., Liu, Y., Zou, B., King, G. P., et al. (2018). Oceanic eddy characteristics and generation mechanisms in the Kuroshio Extension region. *Journal of Geophysical Research: Oceans*, *123*(11), 8548–8567. https://doi.org/10.1029/2018jc014196

Liu, Y., Dong, C., Liu, X., & Dong, J. (2017). Antisymmetry of oceanic eddies across the Kuroshio over a shelfbreak. *Scientific Reports*, *7*(1), 1–7. https://doi.org/10.1038/s41598-017-07059-1

Marshall, J., Adcroft, A., Hill, C., Perelman, L., & Heisey, C. (1997). A finite-volume, incompressible Navier Stokes model for studies of the ocean on parallel computers. *Journal of Geophysical Research*, *102*(C3), 5753–5766. https://doi.org/10.1029/96jc02775

Maximenko, N., & Niiler, P. (2006). Mean surface circulation of the global ocean inferred from satellite altimeter and drifter data. In *Proceeding of the Symposium on 15 years of Progress in Radar Altimetry* (Vol. 614). Eur. Space Agency Spec. Publ., ESA SP.

Penven, P., Halo, I., Pous, S., & Marié, L. (2014). Cyclogeostrophic balance in the Mozambique Channel. *Journal of Geophysical Research: Oceans*, *119*(2), 1054–1067. https://doi.org/10.1002/2013jc009528

Qiu, C., Huabin, M., Yanhui, W., Jiancheng, Y., Danyi, S., & Shumin, L. (2019). An irregularly shaped warm eddy observed by Chinese underwater gliders. *Journal of Oceanography*, *75*(2), 139–148. https://doi.org/10.1007/s10872-018-0490-0

Rocha, C. B., Gille, S. T., Chereskin, T. K., & Menemenlis, D. (2016). Seasonality of submesoscale dynamics in the Kuroshio Extension. *Geophysical Research Letters*, *43*(21), 304–311. https://doi.org/10.1002/2016GL071349

Scott, R. M., Pickart, R. S., Lin, P., Münchow, A., Li, M., Stockwell, D. A., & Brearley, J. A. (2019). Three-dimensional structure of a Cold-Core Arctic Eddy interacting with the Chukchi Slope Current. *Journal of Geophysical Research: Oceans*, *124*(11), 8375–8391. https://doi.org/10.1029/2019jc015523

Shakespeare, C. J. (2016). Curved density fronts: Cyclogeostrophic adjustment and frontogenesis. *Journal of Physical Oceanography*, *46*(10), 3193–3207. https://doi.org/10.1175/jpo-d-16-0137.1

Taburet, G., Sanchez-Roman, A., Ballarotta, M., Pujol, M. I., Legeais, J. F., Fournier, F., et al. (2019). DUACS DT2018: 25 years of reprocessed sea level altimetry products. *Ocean Science*, *15*(5), 1207–1224. https://doi.org/10.5194/os-15-1207-2019

Timmermans, M. L., Toole, J., Proshutinsky, A., Krishfield, R., & Plueddemann, A. (2008). Eddies in the Canada Basin, Arctic Ocean, observed from ice-tethered profilers. *Journal of Physical Oceanography*, *38*(1), 133–145. https://doi.org/10.1175/2007jpo3782.1

Torres, H. S., Klein, P., Menemenlis, D., Qiu, B., Su, Z., Wang, J., et al. (2018). Partitioning ocean motions into balanced motions and internal gravity waves: A modeling study in anticipation of future space missions. *Journal of Geophysical Research: Oceans*, *123*(11), 8084–8105. https://doi.org/10.1029/2018jc014438

Uchida, H., & Imawaki, S. (2003). Eulerian mean surface velocity field derived by combining drifter and satellite altimeter data. *Geophysical Research Letters*, *30*(5). https://doi.org/10.1029/2002gl016445

Uchida, H., Imawaki, S., & Hu, J. (1998). Comparison of Kuroshio surface velocities derived from satellite altimeter and drifting buoy data. *Journal of Oceanography*, *54*(1), 115–122. https://doi.org/10.1007/bf02744385

Wenegrat, J. O., & Thomas, L. N. (2017). Ekman transport in balanced currents with curvature. *Journal of Physical Oceanography*, *47*(5), 1189–1203. https://doi.org/10.1175/JPO-D-16-0239.1

Xu, G., Dong, C., Liu, Y., Gaube, P., & Yang, J. (2019). Chlorophyll rings around ocean eddies in the North Pacific. *Scientific Reports*, *9*(1), 1–8. https://doi.org/10.1038/s41598-018-38457-8

Zhang, Z., Qiu, B., Klein, P., & Travis, S. (2019). The influence of geostrophic strain on oceanic ageostrophic motion and surface chlorophyll. *Nature Communications*, *10*(1), 1–11. https://doi.org/10.1038/s41467-019-10883-w

Zhao, M., Timmermans, M. L., Cole, S., Krishfield, R., Proshutinsky, A., & Toole, J. (2014). Characterizing the eddy field in the Arctic Ocean halocline. *Journal of Geophysical Research: Oceans*, *119*(12), 8800–8817. https://doi.org/10.1002/2014jc010488